Chinese Journal of Aeronautics, (2014),27(3): 593–601

Chinese Society of Aeronautics and Astronautics
& Beihang University

Chinese Journal of Aeronautics

cja@buaa.edu.cn
www.sciencedirect.com

Attitude control system design and on-orbit performance analysis of nano-satellite—"Tian Tuo 1"

Ran Dechao, Sheng Tao *, Cao Lu, Chen Xiaoqian, Zhao Yong

College of Aerospace Science and Engineering, National University of Defense Technology, Changsha 410072, China

Received 9 May 2013; revised 1 July 2013; accepted 8 October 2013
Available online 20 November 2013

KEYWORDS

Actuators;
ADCS;
On-orbit performance;
Sensors;
TT-1 nano-satellite

Abstract "Tian Tuo 1" (TT-1) nano-satellite is the first single-board nano-satellite that was successfully launched in China. The main objective of TT-1 is technology demonstration and scientific measurements. The satellite carries out the significant exploration of single-board architecture feasibility validation, and it is tailored to the low-cost philosophy by adopting numerous commercial-off-the-shelf (COTS) components. The satellite is featured with three-axis stabilization control capability. A pitch bias momentum wheel and three magnetic coils are adopted as control actuators. The sun sensors, magnetometers and a three-axis gyro are employed as the measurement sensors. The quaternion estimator (QUEST) and unscented Kalman filter (UKF) method are adopted for the nano-satellite attitude determination. On-orbit data received by ground station is conducted to analysis the performance of attitude determination and control system (ADCS). The results show that the design of ADCS for TT-1 is suitable, robust and feasible.

1. Introduction

With the advantages of small volume, light weight, short development period and low cost, the micro- and nano-satellites have gradually become a new development direction and attracts more and more attention. During the past decades, a tremendous amount of exploration has been done on research and development of micro- and nano-satellites.

On 6th December, 1957, the first nano-satellite Vanguard TV3 was unsuccessfully launched, only a few months after the launch of the first artificial satellite Sputnik-1. In early ages, the main reason for the micro- and nano-satellites was due to the limited payload capabilities of the launch vehicles and the launched satellites were designed and manufactured simply. Once the launch vehicle was able to launch larger weight, satellites became larger and more advanced as well. However, due to the development of low power micro-electronics in the late nineties of last century, this provided a potential way for a high performance over mass ratio.[1] By September 2009, more than 60 micro- and nano-satellites had been launched successfully into space and most of these satellites were developed by universities and the main

* Corresponding author. Tel.: +86 731 84574810.
E-mail addresses: rdcno.11002@163.com (D. Ran), shengtao-2002@163.com (T. Sheng).

Peer review under responsibility of Editorial Committee of CJA.

Production and hosting by Elsevier

1000-9361 © 2014 Production and hosting by Elsevier Ltd. on behalf of CSAA & BUAA. Open access under CC BY-NC-ND license.
http://dx.doi.org/10.1016/j.cja.2013.11.001

objectives of these satellites were technology demonstration, scientific measurements and radio communications, such as TNS-0,[2] STSAT-1,2,[3] MSU-1,[4] TUGSAT-1/BRITE,[5] COMPASS-1,[6] ZDPS-1A.[7]

The attitude determination and control system (ADCS) plays an indispensable part in satellite on-orbit operation which could greatly affect the satellite's performance. The development of micro- and nano-satellite requires an attitude control system that is inexpensive, light-weight, meanwhile with small volume and low power consumption. Therefore, magnetic coils and bias momentum wheel have been adopted as the most popular actuators. Three-axis magnetic coil combined with a pitch bias momentum wheel is a popular way to accomplish the three-axis stabilization control. This method enforces the attitude stabilization in roll and yaw directions by the momentum wheel which is nominally spinning at a fixed rate in the pitch direction of the satellite. Many micro- and nano-satellites operating in the orbit today subject to this control strategy. HAUSAT-2 satellite developed by Space System Research Laboratory (SSRL) uses magnetic torque as an actuator for attitude stabilization and the momentum wheel is used for quick attitude dumping control.[8] ZDPS-1A designed by Zhejiang University also successfully adopts the momentum wheel and magnetic coils as actuators and achieves accurate attitude maintenance.[9]

TT-1 is the first single-board nano-satellite in China, and it is designed and developed by National University of Defense Technology. In the TT-1 design, ADCS plays a crucial role in carrying out the missions including telemetry and control, optical imaging, and space scientific measurement. In the ADCS configuration, the magnetic coils and the momentum wheel are adopted as actuators, and the sun sensors, magnetometers and a three-axis gyro are employed as the measurement sensors.

2. Review of TT-1 nano-satellite mission

2.1. Background of TT-1 nano-satellite

On 10th May, 2012, TT-1 satellite (as shown in Fig. 1) was successfully launched into space from China Taiyuan Satellite Launch Center. The volume of the satellite is 425 mm × 410 mm × 80 mm, and its mass is about 9.3 kg. The satellite is composed of onboard computer (OBC) module, ADCS module, telemetry and control (TTC) module, power system manager (PSM) module, mechanical structure, thermal control module, command execution module, and payloads module.

With potential application of the micro- and nano-satellites, the architecture gradually develops in the direction of modularization and standardization. In terms of exploration of new nano-satellite architecture, TT-1 has also carried out the corresponding efforts. The satellite TT-1 is an innovative nano-satellite designed and developed by using a special architecture. During the design and manufacture of the satellite, a series of key breakthrough has been obtained. Through the integrated electronic design and machine/electric/thermal integration design, the PSM module, the OBC module, the ADCS module and the TTC module are integrated onto a single printed circuit board (PCB). Compared with the conventional satellite, there is no cable connection in TT-1. Consequently, the new single-board architecture greatly reduces the structure

Fig. 1 On-orbit impression of TT-1.

quality and improves the functional density. Moreover, the single board architecture is highly scalable and can be expanded to the standardized and generic functional modular.

TT-1 was also designed to carry out the first experiment of satellite-based automatic identification system (AIS) in China and conduct scientific experiments of atomic oxygen (AO) detection, as well as optical imaging. The lifecycle was originally designed for 30 days. However, up to now, the satellite has been operating on orbit for over one year. Moreover, it pictured out the first AIS map of global ship in China. The whole mission is a complete success.

In summary, the primary missions of TT-1 are as follows:

(1) The validation of single-board nano-satellite architecture.
(2) On-orbit demonstration of the AIS component.
(3) Components/module experiment.
(4) Optical earth imaging.
(5) Space environment detection experiment.

2.2. ADCS scheme

The ADCS is a crucial subsystem in nano-satellite design process. Its performance directly affects the power supply and the telemetry control. The momentum wheel is installed on the pitch axis and provides gyroscopic stiffness for roll and yaw axis stabilization. The magnetic coil installed on the pitch axis is designed as a ring due to the strict volume in this direction, and other two magnetic coils are designed as iron corn configuration. Because of the small volume and low power consumption of TT-1, the momentum wheel is designed to spin at a fixed rate without rate control. The measurement sensors include sun sensors, magnetometers and a three-axis gyro.

The ADCS structure is shown in Fig. 2.

3. ADCS hardware devices for TT-1

3.1. Attitude determination and control objectives

The ADCS begins to operate after the TT-1 separates from the launch vehicle, and it must accomplish several objectives during the lifetime of the satellite.

(1) After separation from the launcher upper stage, the ADCS must start up automatically and seize the initial attitude state.
(2) To dump the initial angular velocity with three-axis magnetic coils.

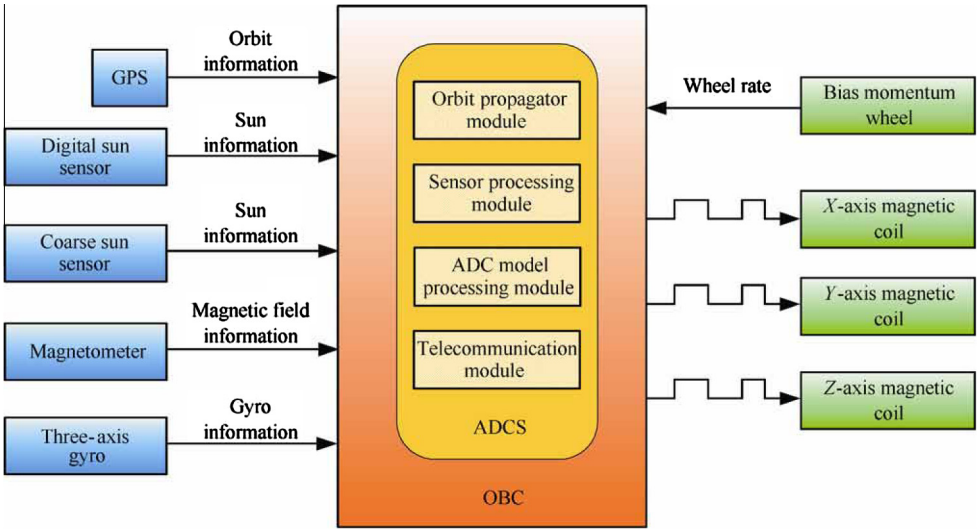

Fig. 2 ADCS structure.

Table 1 Main requirements of ADCS.

ADCS performance	Value
Determination precision (°)	2
Control precision (°)	10
Stabilization precision ((°)/s)	0.1

(3) To determine satellite attitude angle and angular velocity with magnetometer and sun sensor using UKF method.
(4) To achieve three-axis nadir pointing stabilization.

The main performance requirements of ADCS are shown in Table 1.

3.2. ADCS hardware architecture

Sensors and actuators are critical parts for the ADCS. In this subsection, the sensors and actuators used on TT-1 are introduced, such as sun sensors, magnetometers, momentum wheel and magnetic coils. Magnetometers and sun sensors are designed to obtain vector measurements. Sun sensors measure the line-of-sight vector from the spacecraft to the sun, and magnetometers measure the local magnetic field vector. Magnetic coils generate the control torque by interacting with magnetic field, and the momentum wheel stabilizes the attitude through the production of angular momentum with gyroscopic stiffness.

3.2.1. Digital sun sensors

Two digital sun sensors (DSSs) are selected for TT-1 attitude determination system, as shown in Fig. 3. The DSS can determine the angle between the normal direction of solar array and the sun vector. In the current design, two digital sun sensors are installed separately along $+X$-axis and $+Y$-axis. The body reference frame is shown in Fig. 4. The sensors are tolerant to earth albedo in lower Earth orbit (LEO) under a wide range of lighting conditions. The sensor has $\pm 60° \times \pm 60°$ field of view coverage and the measurement accuracy is in the range of 0.5°.

Fig. 3 Digital sun sensor.

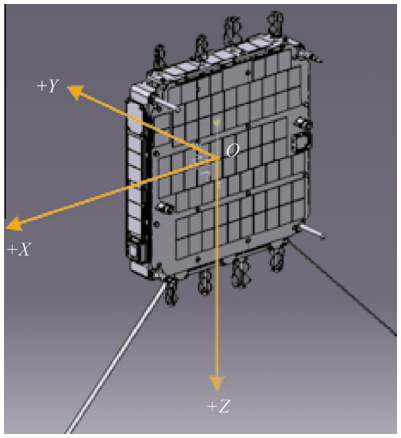

Fig. 4 Body reference frame.

Each sensor consumes less than 0.1 W of power. The projection position of sun vector varies due to the sunlight incident angle. The sunlight detector is installed on the projection plane and can generate current signal according to the incidence

angle of the sunlight. After the satellite turns into three-axis stabilization control mode, the angle between $+Y$-axis and sun vector is about 60°. Thus, the sunlight will appear at the edge of the sensor view field once the satellite exits the eclipse. Note that the sensor with lower angle measurement will be selected for attitude determination if both two sensors get the measurement information.

3.2.2. Coarse sun sensors

Besides the digital sun sensors, a coarse sun sensor is installed on the $+Z$ surface. At the same time, the solar arrays using a mix of Gallium-Arsenide solar cells installed on the $\pm X$, $\pm Y$ and $-Z$ surfaces are also used to measure the sun vector. The sun cells generate current as a function of light intensity and incidence angle to the light source. The relationship between the photocurrent and sunlight intensity can be describe by cosine curve. Thus, each solar array cell can be equal to a coarse sun sensor, and at least one coarse sun sensor can detect the sunlight during the sunlight period. With the power controller installed on the satellite, the sunlight incident angle can be calculated via detecting the current generating by solar cells. However, due to the temperature effect and the measurement noises, this method cannot obtain high measurement accuracy. Thus, the coarse sun sensors are applied as redundant sensors to ensure reliability.

3.2.3. Gyro

The gyro sensor for TT-1 is composed of three gyroscopes along three axes. Each gyroscope can measure the angular velocity around a single axis. The dynamic range of each gyroscope is ± 75 (°)/s with the temperature range of -40 °C to 85 °C. The measurement accuracy of the gyro sensor is in the range of 0.5 (°)/s. Due to the low measurement accuracy, the three-axis gyro is applied for the estimation of the angular velocity at the separation moment and used to judge the validity of the damping control algorithm.

3.2.4. Magnetometers

The magnetic field is another effective vector for attitude determination, and it is the main reference vector for attitude determination in eclipse. The magnetic component vector in the body frame is obtained directly from the magnetometers.[10] Two three-axis magnetometers (TAMs) are installed on the satellite to measure the magnetic vector. The main magnetometer selected for TT-1 is a commercial magnetometer designed by Honeywell, as shown in Fig. 5. Its measurement range is from -2 G to 2 G with the precision 6.7 nT. There is another magnetometer installed in the gyro. However, due to the low measurement precision, this magnetometer is applied as redundant device. Once the main magnetometer cannot work, the redundant magnetometer would substitute as the magnetic field sensor.

3.2.5. Momentum wheel

A pitch bias momentum wheel is utilized as attitude control actuator for TT-1, as shown in Fig. 6. In construction, the momentum wheel consists of a flywheel, bearing assembly and electric drive motor. There is also electronics for driving the wheel, controlling and measuring the wheel speed. The wheel is based on a DC micro-motor. The motor is capable of reaching up to 8200 r/min, depending on voltage supply, with a nominal torque of 6.92 mN·m/A and the fixed rate is around 6100 r/min. The wheel moment of inertia is 1.4×10^{-5} kg·m^2 with 42 mm in diameter and 6 mm in thickness.

The momentum wheel is installed along Y-axis, and it will produce angular momentum continuously. The momentum wheel provides Y-axis stabilization with gyroscopic effect and makes Y-axis point at the normal direction of the orbit plane.

3.2.6. Magnetic coils

Active magnetic control is designed for TT-1. Three magnetic coils are installed along three inertia axes. Two magnetic coils designed in iron corn configuration are installed along the X-axis and Z-axis, and a magnetic ring is installed along Y-axis due to the strict volume, as shown in Fig. 7. The magnetic ring is constructed with 510 turns of copper wire and can provide a maximum dipole of 1.2 A/m^2. The maximum dipole provided by the iron corn magnetic coil is 2 A/m^2.

From Fig. 7, it can be seen that the magnetometer is located near to the magnetic components, such as the motors and the magnetic coils. To improve the measurement accuracy of the magnetometer, the magnetic coils operate at different time periods with the magnetometer. However, due to the need of obtaining a strong magnetic field with small device, a high magnetic permeability material has been exploited as the coil core, and this would lead to severe effect on the magnetometer. Thus, the position of the magnetometers has also been considered with optimization. To reduce the remanent effect of magnetic coils, the magnetometer is installed in the diagonally direction of magnetic coils. Moreover, TAM ground tests and pre-launch calibration are introduced to improve magnetometer measurement accuracy.

Fig. 5 Main magnetometer.

Fig. 6 Momentum wheel.

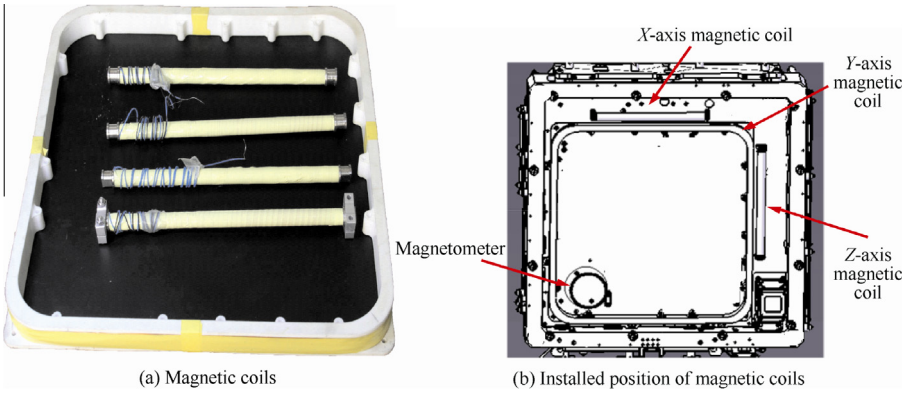

Fig. 7 Magnetic coils and the installed position.

4. Attitude determination and control algorithm for TT-1

In this section, we will introduce the algorithms used on TT-1 to estimate and control its attitude with sensors and actuators. First, we introduce the attitude dynamics equation for the satellite, and then we present the attitude determination and control algorithm, respectively.

4.1. Attitude dynamics

The attitude dynamics of rigid spacecraft with fly wheels can be described as

$$\boldsymbol{J}\dot{\boldsymbol{\omega}}_{\mathrm{bi}} = -\boldsymbol{\omega}_{\mathrm{bi}}^{\times}(\boldsymbol{J}\boldsymbol{\omega}_{\mathrm{bi}} + \boldsymbol{H}) - \dot{\boldsymbol{H}} + \boldsymbol{T}_{\mathrm{c}} + \boldsymbol{T}_{\mathrm{d}} \tag{1}$$

$$\boldsymbol{\omega}_{\mathrm{bi}} = \boldsymbol{\omega}_{\mathrm{bo}} + \boldsymbol{A}_{\mathrm{bo}}\boldsymbol{\omega}_{\mathrm{oi}} \tag{2}$$

where $\boldsymbol{\omega}_{\mathrm{bi}}$ is the angular velocity expressed in the body reference frame, $\boldsymbol{J}$ the inertia matrix, $\boldsymbol{H}$ the angular momentum of the momentum wheel, $\boldsymbol{T}_{\mathrm{c}}$ the control torque vector generated by actuators, $\boldsymbol{T}_{\mathrm{d}}$ external disturbance torque vector imposed on the satellite, $\boldsymbol{\omega}_{\mathrm{bi}}^{\times}$ the skew-symmetric matrix, $\boldsymbol{\omega}_{\mathrm{bo}}$ the angular velocity relative to the orbit reference frame expressed in the body reference frame, $\boldsymbol{\omega}_{\mathrm{oi}}$ the orbital angular velocity expressed in the orbit reference frame, and $\boldsymbol{A}_{\mathrm{bo}}$ the transformation matrix from the orbit reference frame to the body reference frame.

4.2. Attitude determination

Satellite attitude is usually expressed in the form of Euler angles or a direction cosine matrix of a quaternion.[9] The quaternion is also a popular form to express the attitude. Scholars have proposed many methods to estimate attitude and various methods have been applied on the satellite mission successfully. In TT-1 mission, there are different methods adopted for attitude determination. After launch separation, the initial attitude state was unknown. Thus, quaternion estimator (QUEST)[11] algorithm was adopted for attitude determination. However, once the satellite turned into three-axis stabilization control mode, the QUEST method would provide the initial attitude state for the filter method, and the QUEST method would be substituted by the unscented Kalman filter (UKF)[12] algorithm as the attitude determination accuracy of QUEST was not favorable.

4.2.1. QUEST algorithm

The QUEST algorithm and the three-axis attitude determination (TRIAD) algorithm are the most commonly used deterministic algorithms for attitude determination. They are both solutions to the Wahaba's problem.[13] The QUEST and TRIAD algorithm have been both utilized successfully on the nano-satellite. For example, the ION[14] nano-satellite (failed launch) planned to use the TRIAD algorithm with magnetometer and sun sensor measurements. The Cute-1.7 + APD II[15] developed by Laboratory for Space Systems at the Tokyo Institute of Technology utilized the QUEST algorithm onboard to estimate the attitude. Due to the low computation burden of QUEST, TT-1 adopted it to seize the initial attitude with magnetometer and sun sensor measurements. Note that once the two vectors are parallel, the measurements obtained at last time interval will be preserved until the unparallel vectors are obtained.

4.2.2. UKF algorithm

UKF algorithm is used for attitude determination in three-axis stabilization phase. The state vector $\boldsymbol{X}$ combines the attitude quaternion $\boldsymbol{q}_{\mathrm{bo}}$ and $\boldsymbol{\omega}_{\mathrm{bi}}$. The system state equation consists of kinematics and dynamics equations, and can be described as follows:

$$\dot{\boldsymbol{X}} = \begin{bmatrix} \boldsymbol{q}_{\mathrm{bo}} \otimes \boldsymbol{Q}(\boldsymbol{\omega}_{\mathrm{bo}})/2 \\ \boldsymbol{J}^{-1}(-\boldsymbol{\omega}_{\mathrm{bi}}^{\times}(\boldsymbol{J}\boldsymbol{\omega}_{\mathrm{bi}} + \boldsymbol{H}) - \dot{\boldsymbol{H}} + \boldsymbol{T}_{\mathrm{c}} + \boldsymbol{T}_{\mathrm{d}}) \end{bmatrix} + \begin{bmatrix} \boldsymbol{I}_{3\times 3} & \boldsymbol{0} \\ \boldsymbol{0} & \boldsymbol{I}_{3\times 3} \end{bmatrix} \begin{bmatrix} \boldsymbol{v}_1 \\ \boldsymbol{v}_2 \end{bmatrix} \tag{3}$$

where $\boldsymbol{v}_1$ and $\boldsymbol{v}_2$ represent Gaussian white noise sequences.

The accuracy of the attitude estimation depends on the precision of all sensors. The measurement model is set up with magnetic field vector $\boldsymbol{B}_{\mathrm{bo}}$ and sun vector $\boldsymbol{S}_{\mathrm{bo}}$. The measurement model in sunlight is described as follows:

$$\boldsymbol{Z}_k = \begin{bmatrix} \boldsymbol{B}_{\mathrm{bo}} \\ \boldsymbol{S}_{\mathrm{bo}} \end{bmatrix} = \begin{bmatrix} \boldsymbol{A}_{\mathrm{bo}}(\boldsymbol{q}_{\mathrm{bo}})\boldsymbol{A}_{\mathrm{oi}}\boldsymbol{A}_{\mathrm{ig}}\boldsymbol{B}_{\mathrm{g}} \\ \boldsymbol{A}_{\mathrm{bo}}(\boldsymbol{q}_{\mathrm{bo}})\boldsymbol{A}_{\mathrm{oi}}\boldsymbol{S}_{\mathrm{i}} \end{bmatrix} + \begin{bmatrix} \boldsymbol{v}_{\mathrm{b}} \\ \boldsymbol{v}_{\mathrm{s}} \end{bmatrix} \tag{4}$$

where $\boldsymbol{B}_{\mathrm{g}}$ and $\boldsymbol{S}_{\mathrm{i}}$ are the magnetic field and sun vector described in the geographic frame and the inertial frame, respectively. $\boldsymbol{A}_{\mathrm{oi}}$ is the transformation matrix from the inertial frame to the orbit frame, and $\boldsymbol{A}_{\mathrm{ig}}$ is the transformation matrix from the geographic frame to the inertial frame. $\boldsymbol{v}_{\mathrm{b}}$ and $\boldsymbol{v}_{\mathrm{s}}$ represent Gaussian white noise sequences. Once the satellite's orbit is in eclipse, effective sun vectors cannot be obtained by the sun sensors. At

this time, only the TAM can be obtained as the measurement vector. More details of UKF algorithm are presented in Ref. [16].

4.3. Attitude control

In TT-1, three magnetic coils combined with a pitch bias momentum wheel are designed to accomplish satellite attitude control. In this subsection, both damping control and three-axis stabilization control algorithms are described in detail.

4.3.1. Damping control

After launch separation, the satellite is assumed in random initial attitude state with large angular velocity. In this phase, only magnetometer can be used as sensors, and the magnetic coils are used as the main actuators for attitude damping control. The main objective of this phase is to reduce the angular velocity with magnetic coils.

B-dot method[17] is the most popular algorithm in this phase due to its fast convergence and low computation burden. However, the B-dot method is severely affected by the magnetometer measurement noise. In order to improve the control precision, the angle between component vector in Y-axis and $\boldsymbol{B}_{\mathrm{bo}}$ is firstly defined as follows:

$$\alpha_y = \arccos \frac{B_y}{\sqrt{B_x^2 + B_y^2 + B_z^2}} \tag{5}$$

where B_x, B_y and B_z are the component vectors of $\boldsymbol{B}_{\mathrm{bo}}$ in X-axis, Y-axis and Z-axis, respectively.

The time derivate of α_y is calculated by the magnetometer measurement at each sample time interval:

$$\dot{\alpha}_y(t_k) = \frac{\alpha_y(t_k) - \alpha_y(t_{k-1})}{t_k - t_{k-1}} \tag{6}$$

The damping control is divided into two phases.

Phase 1: Dump the angular velocity of X-axis and Y-axis with magnetic coils in Y-axis, and establish the Y-Thomson stabilization state. Meanwhile, Y-axis is driven to the normal direction of orbit plane. The component vector of dipole moment $\boldsymbol{M}$ in Y-axis is presented as follows:

$$M_y(t_k) = -k_y \dot{\alpha}_y(t_k) \tag{7}$$

where k_y is the control gain.

Phase 2: Dump the angular velocity of Y-axis with Z-axis or X-axis magnetic coil to a reference angular velocity ω_{ref}. The component vector of $\boldsymbol{M}$ in X-axis or Z-axis is presented as follows:

$$\begin{cases} M_x = k_x(\omega_y - \omega_{\mathrm{ref}})\mathrm{sgn}(B_z) \\ M_z = k_z(\omega_y - \omega_{\mathrm{ref}})\mathrm{sgn}(B_x) \end{cases} \tag{8}$$

where ω_y is the angular velocity of Y-axis, and k_x and k_z are the control gains.

4.3.2. Three-axis stabilization control

After the phase of damping control, the proportional-derivative (PD) control law is adopted to adjust the satellite to the desired orientation. The control law of the magnetic coils is

$$\boldsymbol{T}_{\mathrm{c}} = -\boldsymbol{K}_{\mathrm{p}}\boldsymbol{\Theta} - \boldsymbol{K}_{\mathrm{q}}\boldsymbol{\omega}_{\mathrm{bo}} \tag{9}$$

where $\boldsymbol{K}_{\mathrm{p}}$, $\boldsymbol{K}_{\mathrm{q}}$ are coefficient matrix of the control gains. $\boldsymbol{\Theta} = [\phi, \theta, \psi]^{\mathrm{T}}$ represents the attitude angle, and ϕ, θ and ψ represent roll, pitch and yaw angle, respectively.

As is well known, the dipole moment $\boldsymbol{M}$ of magnetic coils interacts with geomagnetic field $\boldsymbol{B}$ to produce the control torque:

$$\boldsymbol{T}_{\mathrm{c}} = \boldsymbol{M} \times \boldsymbol{B} \tag{10}$$

The constraint dictated by the magnetic coils is that $\boldsymbol{T}_{\mathrm{c}}$ only generates in the orthogonal direction with magnetic field $\boldsymbol{B}$. Consequently, the best control law applied on the magnetic dipole moment is

$$\boldsymbol{M} = (\boldsymbol{B} \times \boldsymbol{T}_{\mathrm{c}})/\|\boldsymbol{B}\|^2 \tag{11}$$

4.3.3. Safe control mode

Safe control mode is very important in attitude control process. Once sever failure occurs or power supply is not sufficient, the satellite will turn into safe control mode state. According to the data stored in the non-volatile memory, this state can be entered at any phase. Once the satellite recovers the power energy, the system will restart. The conditions for each mode to switch are shown in Fig. 8. The switch conditions for each control mode are shown in Table 2.

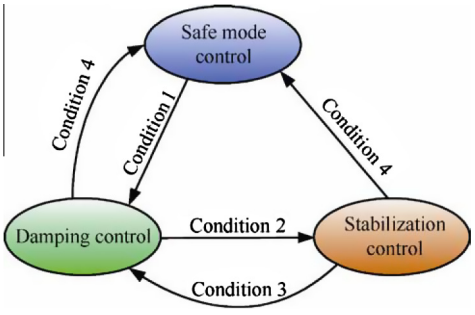

Fig. 8 Attitude control flow chart.

Table 2 Switch conditions for each control mode.

Condition	Switch condition
Condition 1	Launch separation successfully Electric energy sufficient
Condition 2	In sunlight area Attitude angular velocity error: roll/yaw <0.15 (°)/s, pitch <0.35 (°)/s Attitude angular error: roll/yaw $<80°$, pitch $<20°$ Conditions 1, 2 and 3 last for more than 10 s
Condition 3	Attitude angular velocity error over 0.8 (°)/s Condition 1 lasts for more than 10 s
Condition 4	Attitude determination algorithm divergence Electric energy insufficient Ground telemetry command

5. On-orbit data analysis

In this section, data received by ground station is used to analyze the ADCS on-orbit performance of TT-1. The satellite operates in a sun synchronous orbit with the altitude of 480 km, the eccentricity of 0.000454 and the inclination angle of 97.3°. The performances of damping phase and stabilization phase are analyzed, respectively. It can be concluded that the accuracy of three-axis control is about ±10°, and the nadir pointing accuracy can be constrained within ±5°.

5.1. Damping phase

The objective of this phase is to reduce the angular velocity with the damping control strategy. Fig. 9(a) clearly shows the attitude angular velocity after successful launch separation. From Fig. 9(a), we can see that the attitude angular velocity after separation was within 1.5 (°)/s. This demonstrates that the separation design is very successful. Fig. 9(b) shows the momentum wheel speed. After separation, the momentum wheel speeded up rapidly and stabilized at a fixed rate in 10 s. Fig. 9(c) shows the control state after separation. From Fig. 9(c), it can be seen that the control mode was successfully changed from damping control to PD control. The damping control was from 07:19:52 to 07:20:13, which only lasted for 21 s. The damping phase is short and unconspicuous due to the small angular velocity after separation. After that, the attitude control state turned into stabilization control. Fig. 9(d) shows the attitude angular velocity in the second orbit. It is obvious that the attitude angular velocity had been constrained within 0.12 (°)/s. Moreover, the attitude angular velocity ω_x in X-axis and the attitude angular velocity ω_z in Z-axis had converged to the range of ±0.06 (°)/s. This demonstrates that the damping control algorithm is effective and suitable for TT-1 nano-satellite.

5.2. Three-axis stabilization phase

After damping control phase, the satellite turned into the three-axis stabilization control mode. Firstly, the performance of this phase in sunlight area is analyzed. As shown in Fig. 10, the time period is from 06:50:18 to 06:54:29, 14th May, 2012 UTC. From Fig. 10(a), we can conclude that three-axis attitude angle had been constrained within ±6° while the pitch angle was constrained within 3°. Moreover, it is clearly that the pitch angle was more stable than the roll angle and the yaw angle. Thus, it can be concluded that the momentum wheel control in pitch axis is effective. From Fig. 10(b), it can be seen that the attitude angular velocity of roll and yaw axis had converged to the range of ±0.06 (°)/s, and the pitch angular velocity had been constrained within ±0.12 (°)/s. Meanwhile, the wheel speed was stable at about 6100 r/min,

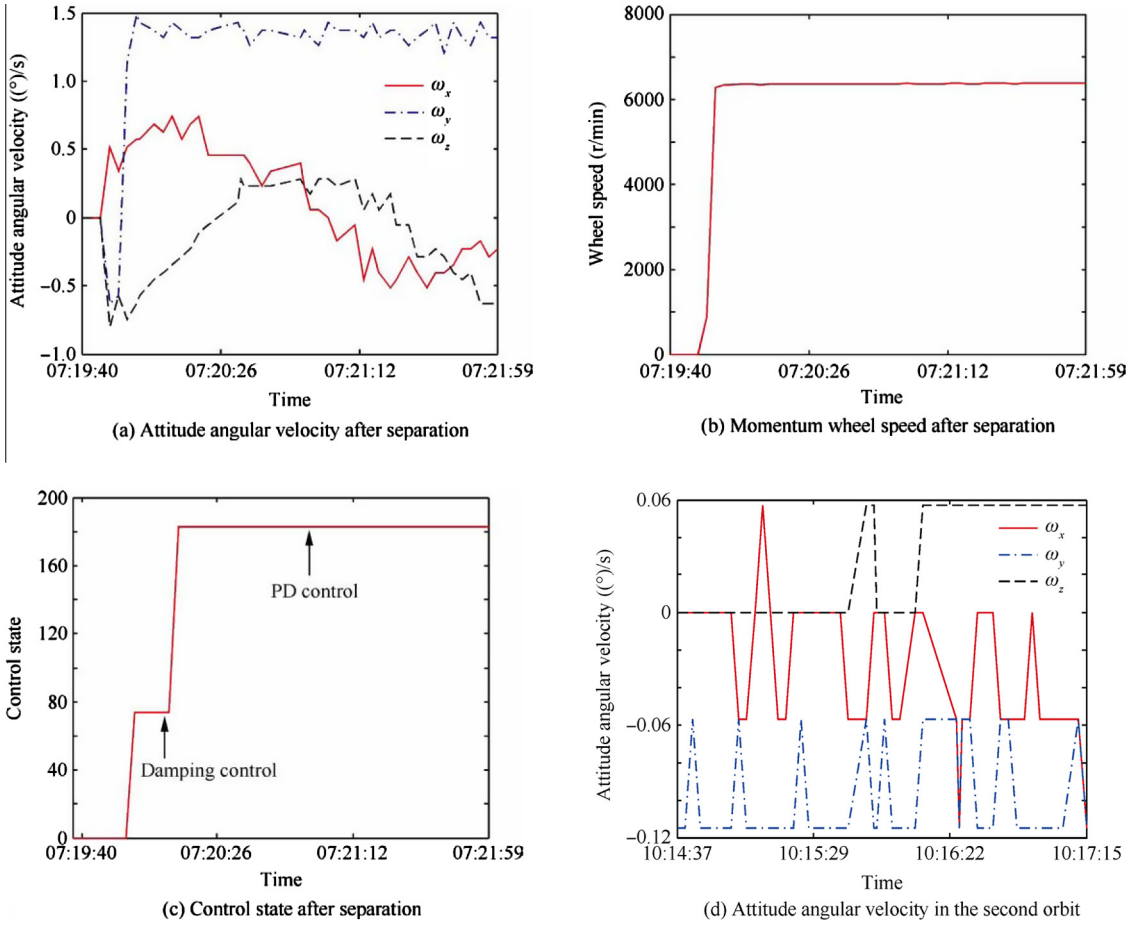

Fig. 9 Damping phase.

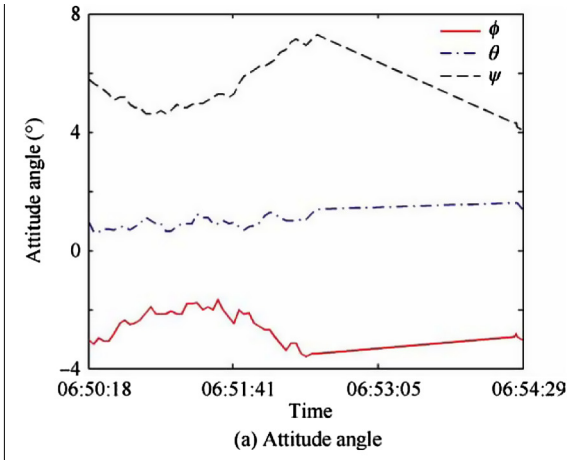

(a) Attitude angle

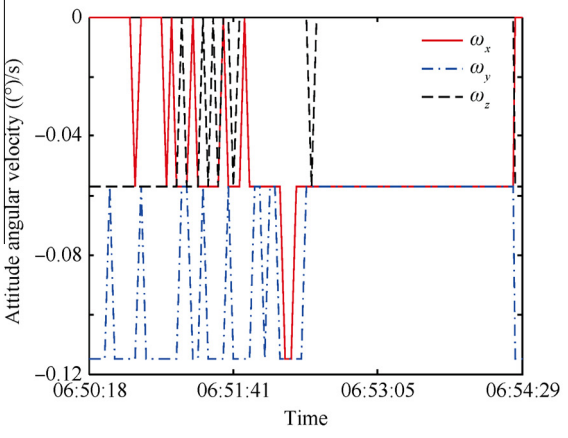

(b) Attitude angular velocity

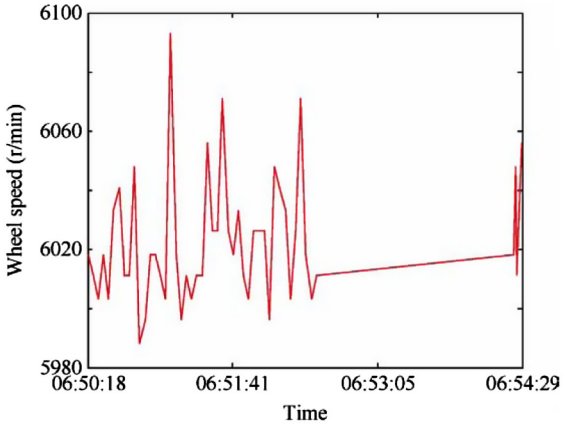

(c) Momentum wheel speed

Fig. 10 On-orbit data during three-axis control in sunlight.

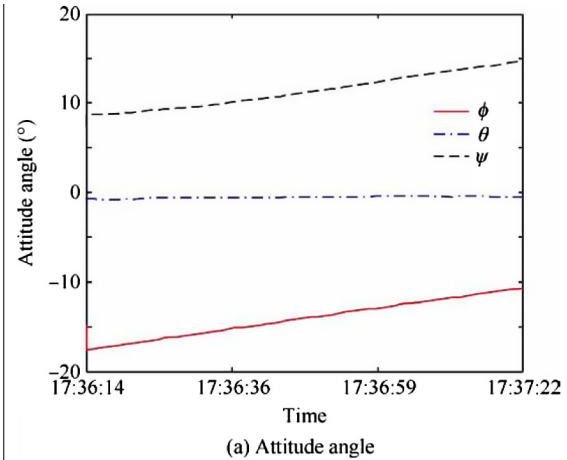

(a) Attitude angle

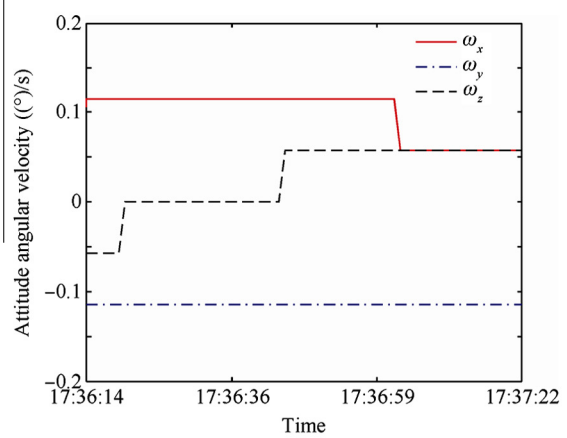

(b) Attitude angular velocity

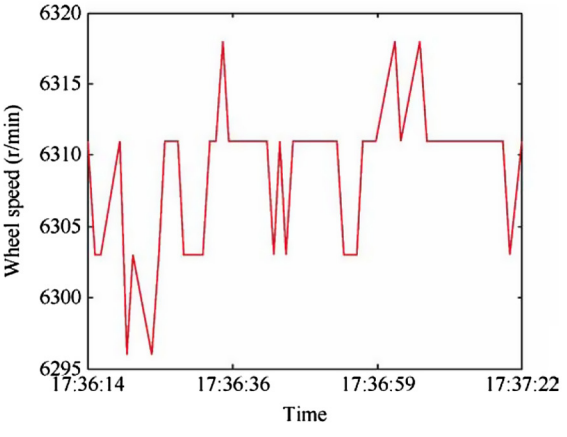

(c) Momentum wheel speed

Fig. 11 On-orbit results during three-axis stabilization phase in eclipse.

as shown in Fig. 10(c). Therefore, it can be concluded that the performance of ADCS is satisfying in sunlight area.

The performance of ADCS in eclipse is shown in Fig. 11. The time period is from 17:36:14 to 17:37:22, 23rd May, 2012 UTC. At that time, the satellite had been sent into space for more than 10 days. In eclipse, the sun sensor cannot generate effective information for attitude determination, and only the magnetometer were obtained as the measurement vector. Thus, the ADCS performance in eclipse would be worse than that in sunlight area. From Fig. 11, it can be obtained that the absolute values of all three attitude angle errors were constrained within 20°, and the pitch attitude angle error was around 5° with slow changes. Meanwhile, the angular velocity of yaw and roll axis were constrained within 0.1 (°)/s, and the pitch attitude velocity was constrained within 0.12 (°)/s. Therefore, we can obtain that the ADCS can also work effectively even in eclipse, and the satellite is also three-axis stable. However, compared with the performance in sunlight area, the control accuracy in eclipse is much worse.

Fig. 12 Image of Earth outline from TT-1 camera.

5.3. Optical camera imaging

Optical imaging has been one of the most popular on-orbit missions for micro- and nano-satellites and this is based on a good attitude control performance. TT-1 is equipped with a reinforced commercial camera module for optical imaging. The maximum pixel resolution of the image is 640×480 (JPEG), and the ground resolution is about 2 km, as shown in Fig. 12. From the picture, it can be concluded that the camera is able to capture the Earth which proves that the ADCS for TT-1 is suitable and effective.

6. Conclusion

TT-1 has been on orbit for over one year which far exceeds one month lifespan, and it has accomplished all the missions successfully. As the first single-board nano-satellite in China, TT-1 verifies the single-board structure and actualizes no cable connection.

In this paper, the design of ADCS subsystem is presented in detail and its on-orbit performance is analyzed. According to the original telemetry data, it can be concluded that the initial design of ADCS for TT-1 is suitable and feasible. In sunlight area, the attitude nadir pointing accuracy is within 5° which is better than the designed accuracy of 10°. In eclipse, ADCS can also work effectively. The favorable attitude control performance guarantees plenteous power supply and optical imagining.

For further study, more suggestions can be concluded through the on-orbit performance analysis of TT-1 mission. To obtain a precise attitude control, variable speed momentum wheel or three-axis reaction wheels control method should be taken into account. In addition, star sensors can be considered to improve ADCS performance in eclipse.

Acknowledgements

The authors thank all the teachers, researchers, engineers and students involved in satellite design for the great effort placed for the success of the TT-1 nano-satellite mission. The authors also thank the reviewers for the useful comments which greatly improve the paper.

References

1. Bouwmeester J, Guo J. Survey of worldwide pico- and nanosatellite missions, distributions and subsystem technology. *Acta Astronaut* 2010;**67**(7–8):854–62.
2. Ovchinnikov MY, Ilyin AA, Kupriynova NV, Penkov VI, Selivanov AS. Attitude dynamics of the first Russian nanosatellite TNS-0. *Acta Astronaut* 2007;**61**(1–6):277–85.
3. Lee JH, Kim SB, Kim KH, Lee SH, Im YJ, Fumin Y, et al. Korea's first satellite for satellite laser ranging. *Acta Astronaut* 2005;**56**(5):547–53.
4. Martinelli MI, Sánchez Peña RS. Passive 3 axis attitude control of MSU-1 pico-satellite. *Acta Astronaut* 2005;**56**(5):507–17.
5. Koudelka O, Egger G, Josseck B, Deschamp N, Cordell Grant C, Foisy D, et al. TUGSAT-1/BRITE-Austria—the first Austrian nanosatellite. *Acta Astronaut* 2009;**64**(11-12):1144–9.
6. Scholz A, Ley W, Dachwald B, Miau JJ, Juang JC. Flight results of the COMPASS-1 picosatellite mission. *Acta Astronaut* 2010;**67**(9–10):1289–98.
7. Yang M, Wang H, Wu CJ, Wang CH, Ding LC, Zheng YM, et al. Space flight validation of design and engineering of the ZDPS-1A pico-satellite. *Chin J Aeronaut* 2012;**25**(5):725–38.
8. Chang YK, Kang SJ, Moon BY, Lee BH. Low-cost responsive exploitation of space by HAUSAT-2 nano-satellite. In: 4th Responsive space conference; 2006 Apr 24-27; Los Angeles, USA. Reston: AIAA; 2006. p. 1-17.
9. Xiang T, Meng T, Wang H, Han K, Jin ZH. Design and on-orbit performance of the attitude determination and control system for the ZDPS-1A pico-satellite. *Acta Astronaut* 2012;**77**:182–96.
10. Springmann JC, Sloboda AJ, Klesh AT, Bennett MW, Cutler JW. The attitude determination system of the RAX satellite. *Acta Astronaut* 2012;**75**:120–35.
11. Shuster MD, Oh SD. Three-axis attitude determination from vector observations. *J Guid Control Dyn* 1981;**4**(1):70–7.
12. Julier SJ, Uhlmann JK. A new extension of the Kalman filter to nonlinear systems. In: *Proc. SPIE 3068, signal processing, sensor fusion, and target recognition VI*; 1997 Apr 21; Orlando, USA. Bellingham: SPIE; 1997.
13. Wahba G. A least squares estimate of spacecraft attitude. *SIAM Rev* 1965;**7**(3):409.
14. Thakker P, Shiroma WA. *Emergence of pico- and nano-satellites for atmospheric research and technology testing*. Reston: AIAA; 2010. pp. 135–173.
15. Ashida H, Fujihashi K, Inagawa S, Miura Y, Omagari K, Miyashita N, et al. Design of Tokyo Tech nano-satellite Cute-1.7+APD II and its operation. *Acta Astronaut* 2010;**66**(9–10):1412–24.
16. Crassidis JL, Markley FL, Cheng Y. Survey of nonlinear attitude estimation methods. *J Guid Control Dyn* 2007;**30**(1):12–28.
17. Meng T, Wang H, Jin ZH, Han K. Attitude stabilization of a pico-satellite by momentum wheel and magnetic coils. *J Zhejiang Univ Sci A* 2009;**10**(11):1617–23.

Ran Dechao received his M.S. degree in College of Aerospace Science and Engineering from National University of Defense Technology, Changsha, China. He is currently a doctoral candidate in College of Aerospace Science and Engineering, National University of Defense Technology. His research interests include variable structure control and spacecraft attitude control.

Sheng Tao received M.S. and Ph.D. degree in College of Mechatronic Engineering and Automation from National University of Defense Technology, Changsha, China. Since 2009, he has been working at College of Aerospace Science and Engineering, National University of Defense Technology. His major technical activities have been in attitude control system design for micro-satellites.